Materials Research Express

INCLUSIVE PUBLISHING TRUSTED SCIENCE
PURPOSE-LED PUBLISHING™

PAPER • **OPEN ACCESS**

Microfluidic synthesis of tetracycline-loaded chitosan nanoparticles for antibiofilm applications

To cite this article: Adei Abouhagger *et al* 2025 *Mater. Res. Express* **12** 115006

View the article online for updates and enhancements.

You may also like

- Small size 2-DOF piezoelectric platform for unlimited locomotion
A eponis, D Mažeika, V Jrnas et al.
- Calibration of the MACHO Photometric System: *VR*, T_{eff}, and BC_V Calibration for Metalpoor Giants
Michael S. Bessell and Lisa M. Germany
- Analysis of measurement system as the mechatronics system
V Giniotis, K T V Grattan, M Rybokas et al.

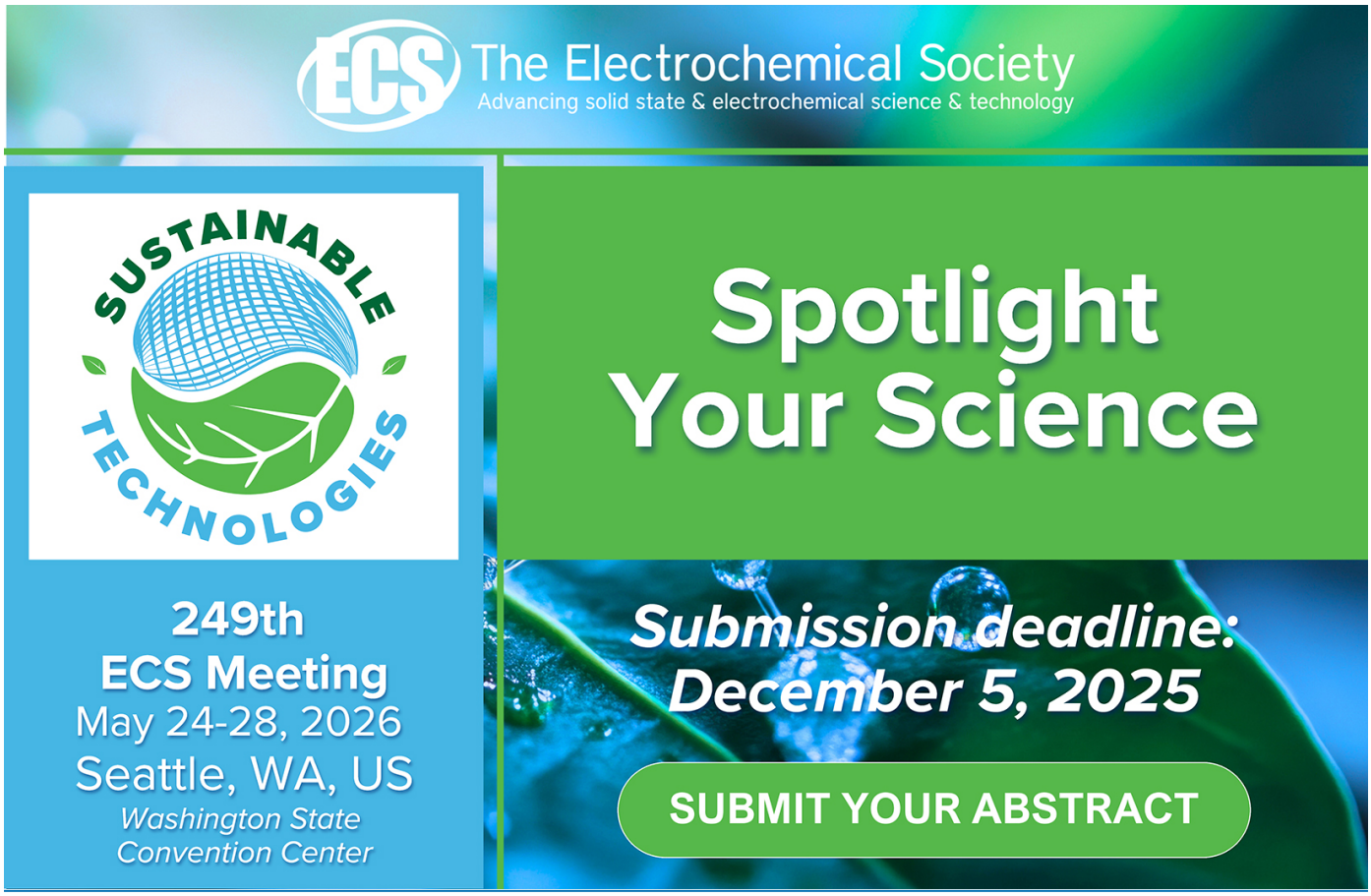

This content was downloaded from IP address 158.129.176.135 on 18/11/2025 at 11:14

Materials Research Express

Check for updates

OPEN ACCESS

RECEIVED
8 August 2025

REVISED
4 November 2025

ACCEPTED FOR PUBLICATION
7 November 2025

PUBLISHED
18 November 2025

Original content from this work may be used under the terms of the Creative Commons Attribution 4.0 licence.

Any further distribution of this work must maintain attribution to the author(s) and the title of the work, journal citation and DOI.

PAPER

Microfluidic synthesis of tetracycline-loaded chitosan nanoparticles for antibiofilm applications

Adei Abouhagger[1,*], Samanta Gelumbickytė[1], Monika Kirsnytė[1], Tatjana Kavleiskaja[2], Arunas Stirkė[1] and Wanessa C M A Melo[1]

[1] Department of Functional Materials and Electronics, State Research Institute Center for Physical Sciences and Technology (FTMC), LT-02300 Vilnius, Lithuania
[2] Department of Polymer Chemistry, Institute of Chemistry, Vilnius University, LT-03225 Vilnius, Lithuania
[*] Author to whom any correspondence should be addressed.

E-mail: wanessa.melo@ftmc.lt

Keywords: microfluidics, chitosan-TPP nanoparticles, drug encapsulation, biofilm disruption, antimicrobial delivery

Supplementary material for this article is available online

Abstract

This study presents a microfluidic approach for synthesizing tetracycline-loaded chitosan–tripolyphosphate (TPP) nanoparticles with tunable physicochemical properties for localized antibiofilm therapy. A custom-designed PDMS chip incorporating sequential micromixing chambers and a serpentine flow region enabled reproducible ionic crosslinking under controlled laminar flow, yielding quasi-spherical nanoparticles (132 ± 3 nm; PDI 0.178 ± 0.004) with a positive surface charge ($+15.8 \pm 0.3$ mV) and 35% drug encapsulation efficiency. FTIR spectroscopy confirmed stable drug incorporation through electrostatic and hydrogen-bonding interactions. Functional assessment against *Staphylococcus aureus* and *Escherichia coli* biofilms demonstrated dose-dependent inhibition of metabolic activity and biomass accumulation. Compared to batch processing, the microfluidic approach enabled more consistent nanoparticle size distribution and improved reproducibility. These findings establish a flow-assisted nanomanufacturing platform for the production of bioactive chitosan-based carriers and highlight their potential in nanoscale therapeutic systems targeting biofilm-associated infections.

1. Introduction

Bacterial biofilms present a major barrier to the effective treatment of chronic and device-associated infections [1]. These structured microbial communities, embedded in a protective extracellular matrix, exhibit enhanced tolerance to antimicrobial agents and environmental stress [2]. Conventional antibiotics often exhibit limited effectiveness against biofilm-associated infections due to rapid clearance, poor tissue penetration [3], and insufficient local concentration at the infection site [4]. This has prompted the development of advanced delivery systems aimed at enhancing drug stability, retention, and localized activity within biofilm environments [5, 6].

Nanoparticle-based antibiotic delivery systems have gained attention for their ability to improve drug solubility, stability, and controlled release [4]. Chitosan, a biocompatible and biodegradable cationic polysaccharide, is particularly well-suited for such systems due to its antimicrobial properties and ability to form nanoparticles through ionic crosslinking with tripolyphosphate (TPP). This mild gelation process enables the formation of stable nanoparticles in aqueous environments, making it suitable for encapsulating therapeutic agents while allowing control over drug release characteristics [7]. However, traditional bulk methods for chitosan nanoparticle fabrication often yield heterogeneous size distributions and suffer from poor reproducibility—factors that limit their translational potential and complicate dosing consistency in biological systems [8].

Microfluidics has emerged as a powerful platform for nanoparticle synthesis [9], offering precise control over fluid dynamics, mixing efficiency, and formulation parameters at the microscale. In microfluidic systems,

© 2025 The Author(s). Published by IOP Publishing Ltd

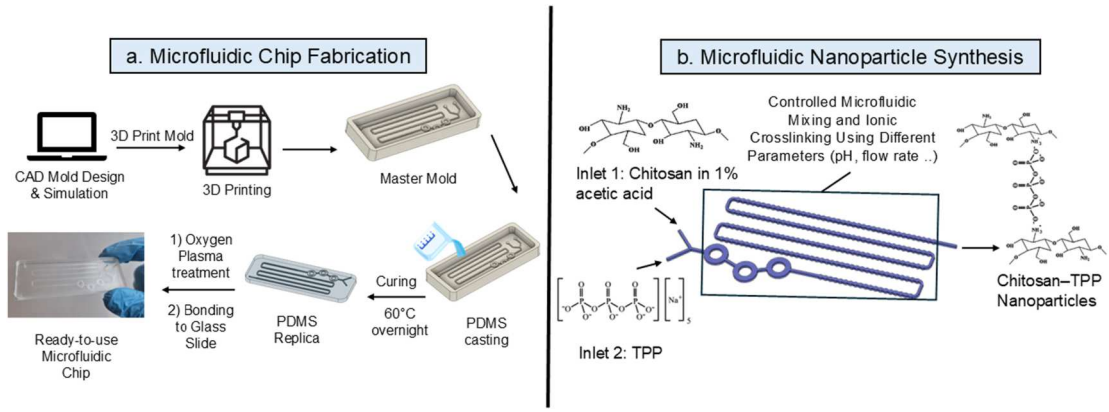

Figure 1. Schematic overview of the experimental workflow. (a) Fabrication of the microfluidic chip using 3D-printed molds and PDMS casting. (b) Microfluidic synthesis of chitosan–TPP nanoparticles.

flow rates, reagent ratios, and channel geometries can be finely tuned to produce nanoparticles with consistent size, charge, and encapsulation characteristics. The laminar flow regime and diffusion-driven mixing enable reproducible and scalable production of well-defined nanoparticles while reducing batch-to-batch variability and reagent consumption [10, 11]. These advantages position microfluidic synthesis as a promising approach for developing nanomedicine formulations with greater process control and quality assurance.

Previous studies have demonstrated the feasibility of microfluidic synthesis for chitosan-based nanoparticles, primarily emphasizing process scalability and physicochemical optimization [12–15]. Building on this foundation, the present work focuses on the microfluidic preparation of tetracycline-loaded chitosan–TPP nanoparticles and investigates how synthesis parameters influence their structural characteristics and antibacterial performance. A custom-designed microfluidic chip with integrated mixing features was developed to enable controlled ionic crosslinking and reproducible nanoparticle formation. Antibiofilm activity was evaluated against *Staphylococcus aureus* and *Escherichia coli* to establish the relationship between nanoparticle properties and biological efficacy. These findings demonstrate the utility of microfluidic synthesis for generating well-defined bioactive nanocarriers and highlight its potential in managing biofilm-associated infections. An overview of the experimental workflow is presented in figure 1.

2. Methods and materials

2.1. Materials

Low molecular weight chitosan (50,000–190,000 Da; viscosity: 20–300 cP, 1 wt % in 1% acetic acid at 25 °C; degree of deacetylation ⩾75%) was obtained from Sigma-Aldrich (USA). Acetic acid and sodium tripolyphosphate (TPP) were also purchased from Sigma-Aldrich and used for nanoparticle preparation. The pH of chitosan solutions was adjusted using 0.5 M sodium hydroxide solution (Sigma-Aldrich, USA). D-mannitol (⩾99%; PanReac AppliChem, Germany; CAS 69-65-8) was used as a cryoprotectant at 5% (w/v) during nanoparticle freeze-drying.

For microfluidic device fabrication, Sylgard™ 184 Silicone Elastomer Kit (Dow Inc., USA) was utilized for PDMS casting. The master mold was fabricated using Zortrax White Resin on a Zortrax Inkspire 3D printer (Olsztyn, Poland), with isopropanol (Sigma-Aldrich, USA) used for post-print cleaning. PTFE tubing with an inner diameter of 1/32″ (Darwin Microfluidics, France) was used for fluid handling. Standard microscope glass slides (1 mm thickness; Thermo Fisher Scientific, USA) served as substrates for chip assembly.

2.2. Microfluidic chip design and fabrication

The microfluidic chip was designed to facilitate efficient passive mixing of chitosan and TPP phases under laminar flow conditions. The layout (figure 2) incorporated three discrete circular mixing chambers (5 mm outer diameter with 3 mm central pillars), followed by a high-aspect-ratio serpentine channel featuring periodic 1 mm expansion zones spaced 0.3 mm apart. This geometry was intended to increase fluid–fluid interface area and residence time, thereby enhancing reagent diffusion and minimizing flow-induced variability during nanoparticle nucleation and growth. The channel network was designed using CAD software, with channel widths of 200 μm and heights of 500 μm, and was optimized for reproducibility, scalability, and compatibility with PDMS soft lithography fabrication.

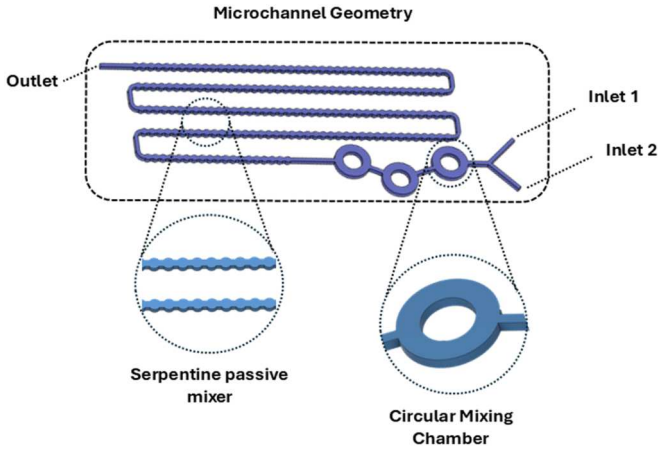

Figure 2. The microfluidic channel layout which includes three circular mixing chambers (5 mm OD, 3 mm pillar) followed by a serpentine channel with periodic 1 mm expansion zones (0.3 mm spacing) to enhance passive mixing under laminar flow.

An overview of the chip fabrication workflow is shown in figure 1(a). Microfluidic molds were fabricated using a Zortrax Inkspire 3D printer with Zortrax white resin. PDMS (Sylgard™ 184, Dow Inc.) was prepared by mixing the elastomer base and curing agent at a 10:1 (w/w) ratio, poured onto the molds, degassed, and cured overnight at 60 °C. After curing, inlet and outlet holes were pierced using a biopsy punch. PDMS replicas were rinsed with isopropanol, dried under a nitrogen stream, and set aside.

Glass microscope slides (1 mm thickness, Thermo Fisher Scientific) were cleaned by immersion in isopropanol followed by 15 min of sonication in a water bath, then dried with nitrogen. Both PDMS and glass substrates were treated using oxygen plasma (Zepto B, Diener Electronic, Germany) at 75% power and 0.35 mbar pressure for 180 s. Immediately after treatment, the substrates were brought into conformal contact to achieve stable and strong bonding. Bonded devices were visually inspected for sealing integrity and absence of leakage, then stored in sterile petri dishes until use.

2.3. NPs synthesis using microfluidic chips

Chitosan–TPP nanoparticles were synthesized via ionic gelation using a custom-fabricated PDMS microfluidic chip. Chitosan was dissolved at 1 mg mL^{-1} in 1% (v/v) acetic acid, and the pH was adjusted to 4.5–5.5 using 0.5 M NaOH, according to the experimental design. TPP was prepared at 1 mg mL^{-1} in distilled water. Both solutions were loaded into separate 10 ml syringes and infused into the chip using syringe pumps (Model ISPLab02, InfuseTek, China). The inlets were connected via PTFE tubing. Chitosan-to-TPP (CS:TPP) flow rate ratios of 2:1, 1.5:1, 1.25:1, and 1:1 were evaluated at a constant total flow rate of 150 μl min^{-1}. Conditions with TPP flow rates exceeding those of chitosan (ratios $<$1:1) were excluded, as they led to rapid gelation, visible precipitation, and channel blockage.

The microfluidic device incorporated three sequential circular mixing chambers followed by a high-aspect-ratio serpentine channel with periodic circular expansion zones to enhance mixing and enable controlled nanoprecipitation. Nanoparticle formation was presumed to initiate within the circular chambers, with further growth and stabilization occurring along the downstream serpentine segment.

The nanoparticle suspension was collected into sterile centrifuge tubes, centrifuged at 13,000 rpm for 20 min, and washed with distilled water. The resulting pellet was redispersed in distilled water via brief sonication and stored at 4 °C prior to freeze-drying and further characterization.

2.3.1. Synthesis of tetracycline-loaded nanoparticles and drug loading optimization

To evaluate drug loading performance, tetracycline hydrochloride was incorporated into the chitosan phase at varying concentrations (16.7–133 μg ml^{-1}) prior to microfluidic synthesis. The tetracycline–chitosan solutions were stirred for 30 min at room temperature to facilitate drug interaction and pre-association with the polymer matrix. All other formulation parameters—including chitosan concentration, pH, CS:TPP flow rate ratio, and total flow rate—were fixed at the optimized values identified during preliminary screening. The drug-loaded nanoparticles were synthesized as described in section 2.3, collected, and centrifuged. The supernatants were analysed to quantify unencapsulated tetracycline and calculate encapsulation efficiency (EE%) and drug loading (DL%) as detailed in section 2.5.3.

2.4. Nanoparticle characterization

2.4.1. Dynamic light scattering (DLS) and zeta potential analysis

The hydrodynamic diameter, polydispersity index (PDI), and zeta potential of the nanoparticles were measured using a Zetasizer Nano ZS (Malvern Panalytical, UK) at 25 °C. Measurements were conducted at a nanoparticle concentration of 1 mg mL^{-1} in distilled water. Each sample was analysed in triplicate, and values are reported as mean ± standard deviation.

2.4.2. Scanning electron microscopy (SEM)

The morphology of freeze-dried nanoparticles was examined using a scanning electron microscope (Hitachi, Japan). Samples were immobilized on carbon adhesive tape mounted on aluminium stubs and sputter-coated with a thin chromium layer (~10 nm) to enhance imaging resolution and contrast. SEM micrographs were acquired at a fixed 50,000× magnification to assess particle size, shape, and surface morphology.

2.4.3. Encapsulation efficiency and drug loading

Encapsulation efficiency (EE%) and drug loading (DL%) of tetracycline were determined using the freshly synthesized nanoparticle suspensions prior to freeze-drying. Samples were centrifuged at 13,000 rpm for 30 min, and the absorbance of the supernatant was measured at 276 nm using a UV–Vis spectrophotometer (Dynamica Scientific Ltd, UK) equipped with 1 cm pathlength quartz cuvettes. The concentration of unencapsulated tetracycline was quantified using a previously established standard calibration curve.

Encapsulation efficiency was calculated using equation (1):

$$EE\% = \left(\frac{C_{initial} - C_{free}}{C_{initial}}\right) \times 100 \quad (1)$$

Drug loading was calculated by freeze-drying 1 ml of nanoparticle suspension and weighing the resulting dry mass. The amount of encapsulated tetracycline was calculated as $C_{encapsulated} = C_{initial} - C_{free}$, and drug loading was determined using equation (2):

$$DL\% = \left(\frac{C_{encapsulated}}{Total\ NPs\ mass}\right) \times 100 \quad (2)$$

2.4.4. Fourier-transform infrared spectroscopy (FTIR)

FTIR analysis was performed to evaluate chemical interactions between chitosan, TPP, and tetracycline, and to confirm successful encapsulation. Spectra were recorded using an Agilent Cary 630 FTIR spectrometer (Agilent Technologies, USA) equipped with an ATR (attenuated total reflectance) module. Spectra were collected in the range of 400–4000 cm^{-1} at a resolution of 4 cm^{-1}, and averaged over 100 scans per sample. Background correction was applied before each measurement. Samples were analysed in lyophilized powder form.

2.5. Biofilm formation and treatment

Biofilms of *S. aureus* (ATCC 25923) and *E. coli* (K12, DMS 498) were established in sterile, flat-bottom 96-well plates. Each well was filled with 150 µl of brain heart infusion (BHI) broth inoculated with an overnight culture diluted to an optical density of 0.05 at 600 nm (OD_{600}). Plates were incubated at 37 °C for 24 h under mild agitation (50 rpm) on an orbital shaker to promote biofilm formation.

Following incubation, planktonic cells were gently removed, and the wells were washed three times with sterile phosphate-buffered saline (PBS, pH 7.4) to eliminate waste and non-adherent bacteria. Biofilms were then treated by adding 150 µl of fresh BHI broth containing different concentrations of tetracycline-loaded nanoparticles. Plates were incubated for an additional 24 h at 37 °C.

After treatment, wells were washed again three times with PBS to remove residual media and planktonic cells. The treated biofilms were then subjected to further quantification using the XTT and crystal violet assays, as described in the following subsections.

2.5.1. XTT metabolic activity assay

The metabolic activity of the microbial biofilms was assessed using the Cell Proliferation Kit (XTT) (Roche, Switzerland). A working solution was prepared by mixing the XTT labelling reagent with the electron-coupling reagent in a 50:1 ratio. Then, 50 µl of the XTT mixture was added to each well, and the plate was incubated at 37 °C in the dark for 30 min. Absorbance was measured at 450 nm with a reference wavelength of 620 nm using a Sunrise microplate reader (Tecan Life Sciences, Switzerland). Untreated biofilms and biofilms treated with free tetracycline served as negative and positive controls, respectively. All conditions were tested in triplicate, and results were expressed as mean ± standard deviation.

Table 1. Physicochemical properties of chitosan–TPP nanoparticles synthesized via microfluidic mixing at 150 μl min^{-1}. Z-average diameter, PDI, and zeta potential were measured at 1 mg mL^{-1} in distilled water (mean of triplicates). 'Observations' denote qualitative macroscopic appearance immediately after synthesis (e.g., turbidity, sedimentation, clumping).

Sample ID	pH	CS:TPP flow ratio	CS:TPP molar ratio	Z-average (nm)	PDI	Zeta potential (mV)	Observations
N1	4.5	2:1	4.57:1	257 ± 10.0	0.369 ± 0.007	+6.5 ± 0.1	Aggregations formed
N2	4.5	1.5:1	3.72:1	233 ± 7.0	0.322 ± 0.003	+11.1 ± 0.5	Mild aggregation
N3	4.5	1.25:1	3.19:1	164 ± 2.0	0.279 ± 0.008	+11.2 ± 0.16	Slight turbidity
N4	5	2:1	4.57:1	132 ± 3.0	0.178 ± 0.004	+15.8 ± 0.3	Clear
N5	5	1.5:1	3.72:1	210 ± 12.0	0.227 ± 0.003	+11.5 ± 0.19	Clear
N6	5	1.25:1	3.19:1	193 ± 3.0	0.225 ± 0.004	+9.6 ± 0.3	Aggregates formed
N7	5.5	2:1	4.57:1	159 ± 4.0	0.160 ± 0.002	+12.8 ± 0.1	Clear
N8	5.5	1.5:1	3.72:1	202 ± 10.0	0.278 ± 0.006	+11.1 ± 0.3	Mild aggregation
N9	5.5	1.25:1	3.19:1	188 ± 4.0	0.255 ± 0.005	+9.6 ± 0.5	Aggregates formed

2.5.2. Crystal violet biomass quantification

To quantify total biofilm biomass, the crystal violet (CV) staining assay was performed. After washing the wells with PBS, the biofilms were fixed with 100 μl of 99% methanol for 15 min and allowed to air dry. Wells were then stained with 0.1% (w/v) crystal violet solution for 15 min at room temperature. Excess dye was removed by rinsing the wells three times with distilled water. The bound dye was solubilized with 150 μl of 33% (v/v) acetic acid per well, and absorbance was measured at 590 nm using a microplate reader. All measurements were performed in triplicate.

3. Results

3.1. Microfluidic chip design and fabrication

The microfluidic chip fabrication process yielded defect-free and optically transparent devices with reproducible structural integrity. Oxygen plasma treatment ensured strong bonding between PDMS and glass substrates, with no observable leakage or channel delamination during nanoparticle synthesis experiments. Visual inspection confirmed proper alignment and sealing of all inlets and outlets. All fabricated chips supported stable flow under the tested operational parameters, demonstrating reliable performance and reproducibility across batches during multiple synthesis runs. These results validated the suitability of the chip design and fabrication approach for continuous, laminar-flow-driven nanoparticle production.

3.2. Nanoparticle formation and optimization

The physicochemical properties of chitosan–TPP nanoparticles are known to depend strongly on formulation parameters such as pH and the chitosan-to-TPP ratio. These factors influence ionic crosslinking efficiency and, consequently, particle size, distribution, and stability. To identify suitable conditions for nanoparticle formation, a series of formulations were synthesized using a microfluidic approach and evaluated for their size, polydispersity, and surface charge.

Several chitosan–TPP nanoparticle formulations (N1-9) were synthesized using varying pH values and CS: TPP flow ratios, while maintaining a constant chitosan concentration (1 mg mL^{-1}), TPP concentration (1 mg mL^{-1}), and a total flow rate of 150 μl min^{-1}. The resulting formulations, along with their physicochemical properties and visual stability assessments, are summarized in table 1. Nanoparticles were characterized by dynamic light scattering and zeta potential measurements, and their colloidal characteristics was assessed visually.

Z-average diameters ranged from 132 ± 3 nm to 257 ± 10 nm, with the smallest particles observed at pH 5.0 and 2:1 flow ratio (Sample N4). The polydispersity index (PDI) values indicated generally narrow size distributions, with the lowest PDI of 0.160 ± 0.002 achieved at pH 5.5 (Sample N7), suggesting high formulation homogeneity. Several formulations (e.g., N4, N5, N7) showed clear and stable suspensions, indicating favourable nanoparticle stability. In contrast, formulations with low pH or high TPP content (e.g., N1, N6, N9) exhibited lower colloidal stability, precipitation, and aggregation, which correlated with lower zeta potentials and higher PDI values.

Zeta potential values varied between +9.6 ± 0.3 and +15.8 ± 0.3 mV. Formulations exhibiting surface charges above +11 mV, such as N4 and N7, showed enhanced colloidal stability, aligning with their low PDI values and favourable visual characteristics. Sample N4 (pH 5.0, 2:1 flow ratio) was chosen for subsequent drug

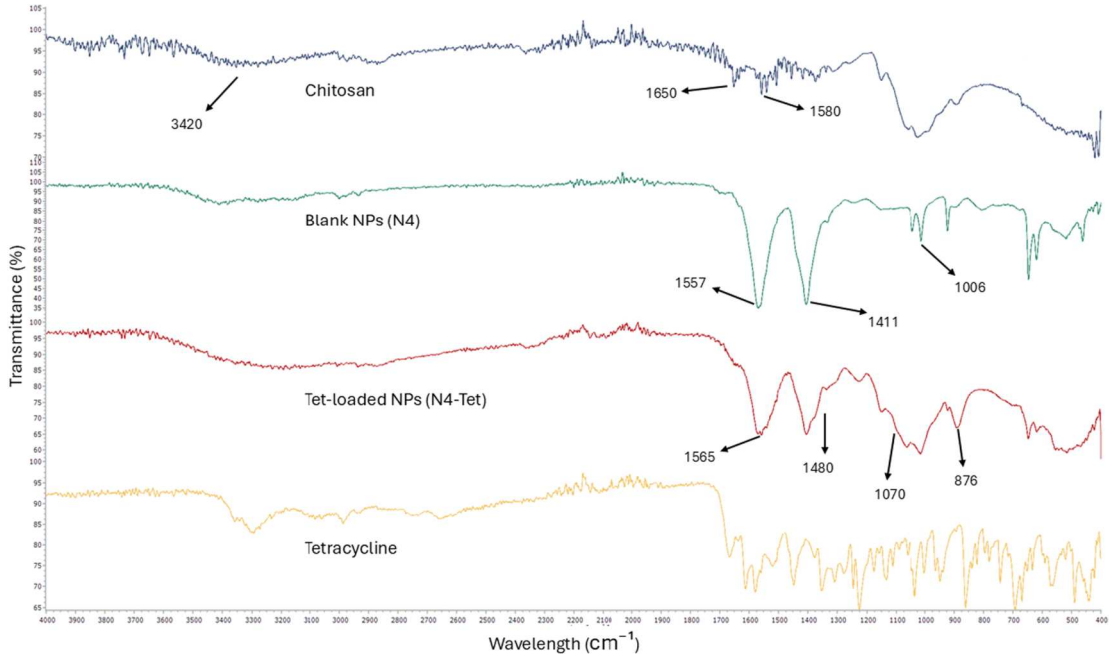

Figure 3. FTIR spectra of chitosan, blank nanoparticles (N4), tetracycline-loaded nanoparticles (N4–Tet), and free tetracycline. The chitosan spectrum shows characteristic peaks at ~3420 cm^{-1} (O–H/N–H stretching), 1650 cm^{-1} (amide I), and 1580 cm^{-1} (amide II). Spectral changes in the blank NPs confirm ionic crosslinking with TPP (1557, 1411, 650, 625 and 1006 cm^{-1}). The N4–Tet spectrum reveals additional peaks at 1480, 1070, and 876 cm^{-1}, indicating successful incorporation of tetracycline. The spectrum of free tetracycline is included for reference.

loading, detailed characterization, and biological assays based on its favourable properties, including minimal particle size and narrow size distribution.

3.3. FTIR spectral analysis of CS-TPP nanoparticles

FTIR spectroscopy was used to characterize the chemical composition and confirm both nanoparticle formation and drug loading (figure 3). The spectrum of raw chitosan exhibited typical bands at ~3420 cm^{-1} (O–H and N–H stretching), 1650 cm^{-1} (amide I, C = O stretching), and 1580 cm^{-1} (amide II, N–H bending), reflecting the polysaccharide's primary amine and hydroxyl groups. In the blank nanoparticles (N4), a distinct band at 1557 cm^{-1} corresponding to $-NH_3^+$ asymmetric stretching emerged, indicating electrostatic interaction with TPP. Additional bands at 1411 and 1006 cm^{-1} were attributed to symmetric $-COO^-$ stretching and P–O bending vibrations, confirming successful crosslinking via ionic gelation. Notably, low-intensity peaks appeared at approximately 650 and 625 cm^{-1}, which were not present in the spectrum of raw chitosan. These peaks likely correspond to P–O bending vibrations, indicating successful incorporation of TPP during nanoparticle formation.

3.4. Morphology of nanoparticles by SEM

SEM was employed to examine the surface morphology and structural features of the optimized chitosan–TPP nanoparticles (N4) and raw chitosan powder (figure 4). The micrograph of sample N4 revealed well-distributed, quasi-spherical nanoparticles with relatively smooth surfaces and sizes predominantly below 130 nm, consistent with DLS measurements. In contrast, the raw chitosan sample displayed an irregular, flaky morphology with dense aggregates and no visible nanoscale features. These observations confirm the successful transformation of bulk chitosan into quasi-spherical nanoparticles via microfluidic ionic gelation.

3.5. Drug encapsulation and loading efficiency

The influence of tetracycline concentration on encapsulation efficiency (EE%) and drug loading (DL%) was evaluated by increasing the total drug input from 16.7 to 133 μg ml^{-1} (figure 5). EE% increased with rising drug concentration, reaching a maximum of approximately 35% at 66.7 μg ml^{-1}, followed by a pronounced decline at higher concentrations. This trend suggests that the chitosan–TPP matrix becomes saturated beyond this threshold, limiting further drug encapsulation.

In contrast, DL% showed a continuous increase up to 66.7 μg ml^{-1}, peaking at 2.24%, and then gradually declined at higher drug inputs. The divergence between EE% and DL% beyond the saturation point reflects a

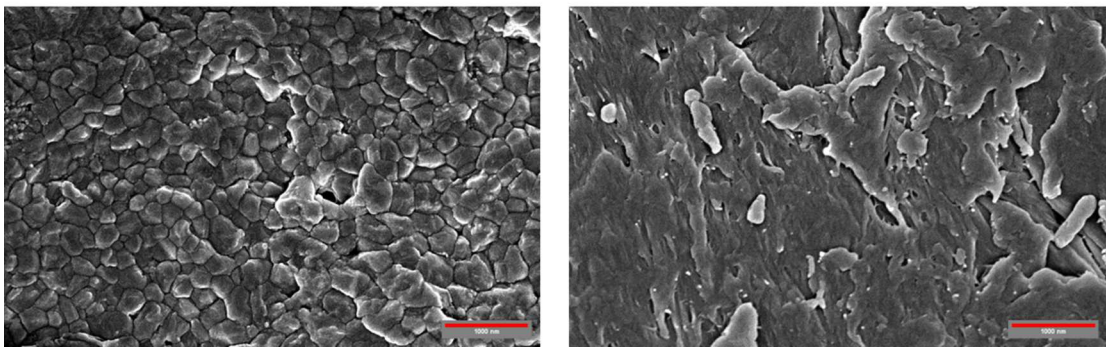

Figure 4. SEM micrographs of (a) chitosan–TPP nanoparticles (N4 formulation) and (b) raw chitosan powder, both captured at 50,000× magnification. The nanoparticles exhibit a quasi-spherical morphology with diameters below 150 nm, while the raw chitosan shows irregular, aggregated structures without visible nanoscale features. Scale bar: 1000 nm.

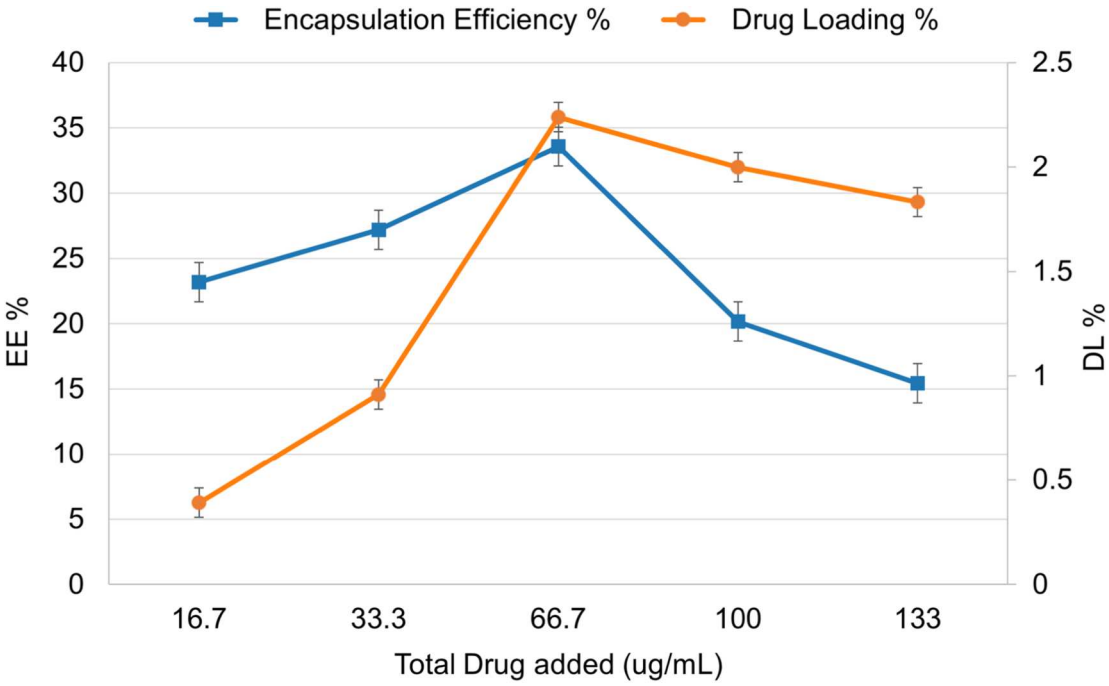

Figure 5. Effect of total tetracycline concentration on encapsulation efficiency (EE%) and drug loading (DL%) of chitosan–TPP nanoparticles synthesized via microfluidics. EE% (blue line) and DL% (orange line) were calculated at increasing input drug concentrations. Data represent mean ± SD (n = 3).

typical limitation in polymer-based nanoparticle systems, where excess drug remains unencapsulated, leading to reduced efficiency and modest gains in loading capacity.

All drug-loading experiments were performed using the optimized formulation parameters from Sample N4 (pH 5.0, CS:TPP ratio 2:1, total flow rate 150 μl min^{-1}). Based on this profile, the formulation with 66.7 μg ml^{-1} of added tetracycline was selected for subsequent biological testing due to its optimal balance between EE% and DL%.

Following tetracycline loading, DLS analysis revealed an increase in the hydrodynamic diameter of the optimized N4 formulation from 132 ± 3 nm to 197 ± 19 nm, reflecting drug incorporation within the nanoparticle matrix. Following tetracycline encapsulation, the polydispersity index (PDI) remained low (0.160 ± 0.002), and the zeta potential slightly decreased from +15.8 ± 0.3 mV to +13.1 ± 0.4 mV, indicating that the observed increase in particle size did not compromise size uniformity or colloidal stability.

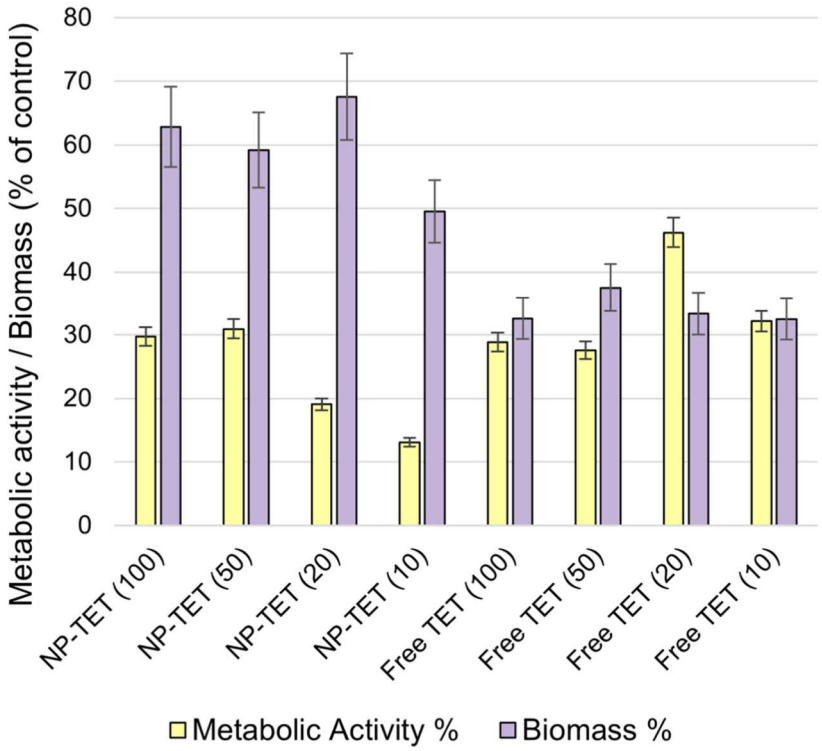

Figure 6. *S. aureus* biofilm response to NP-TET and free TET treatments. Relative metabolic activity and biomass were evaluated after 24 h exposure to tetracycline-equivalent concentrations of 10–100 μg ml^{-1}. Metabolic activity was measured using the XTT assay, and biofilm biomass was quantified by crystal violet (CV) staining. Data are expressed as percentages relative to untreated control biofilms (set as 100%), where lower values indicate inhibition of biofilm growth or metabolic activity. Error bars represent mean ± SD from triplicate measurements.

3.6. FTIR spectral analysis of loaded tetracycline CS-TPP nanoparticles (N4-TET)

Following tetracycline encapsulation (N4–Tet), further spectral modifications were observed (figure 3). The shift of the N–H bending band to 1565 cm^{-1} suggests altered hydrogen bonding or electrostatic interaction with the drug. Distinct absorption bands at 1480, 1070, and 876 cm^{-1}, not present in either chitosan or blank nanoparticles, correspond to characteristic vibrations of tetracycline, including aromatic ring stretching and C–O skeletal modes. These peaks, also present in the free drug spectrum, further verify successful incorporation of tetracycline into the chitosan–TPP matrix. These peaks are consistent with those reported for pure tetracycline, particularly in the regions associated with C = C and ring deformation vibrations [16], and confirm successful loading of the drug within the chitosan–TPP matrix.

3.7. Antibiofilm activity evaluation

The antibiofilm efficacy of free tetracycline (TET) and TET-loaded nanoparticles (NP-TET) was evaluated against biofilms of *S. aureus* and *E. coli*. Metabolic activity and biomass were quantified using the XTT reduction and crystal violet assays, respectively. Treatments were applied at 5–100 μg ml^{-1} (TET equivalent), a range selected from previous antibiofilm studies to span sub-inhibitory to inhibitory concentrations for these tetracycline-susceptible strains [17, 18]. Results for each species are presented below, normalized to untreated control biofilms (defined as 100%).

3.7.1. S. aureus *biofilms*

As shown in figure 6, NP-TET treatment resulted in a concentration-dependent reduction in metabolic activity at concentrations of 100 to 10 μg ml^{-1}, with values decreasing to 29.78 ± 2.12%, 30.95 ± 2.42%, 19.05 ± 1.85%, and 13.08 ± 0.77% for NP-TET at 100, 50, 20, and 10 μg ml^{-1}, respectively. In comparison, free tetracycline treatments resulted in metabolic activities of 28.86 ± 2.30%, 27.54 ± 2.56%, 46.23 ± 3.33%, and 32.19 ± 2.50% at the corresponding concentrations. Notably, at 20 and 10 μg ml^{-1}, NP-TET led to stronger

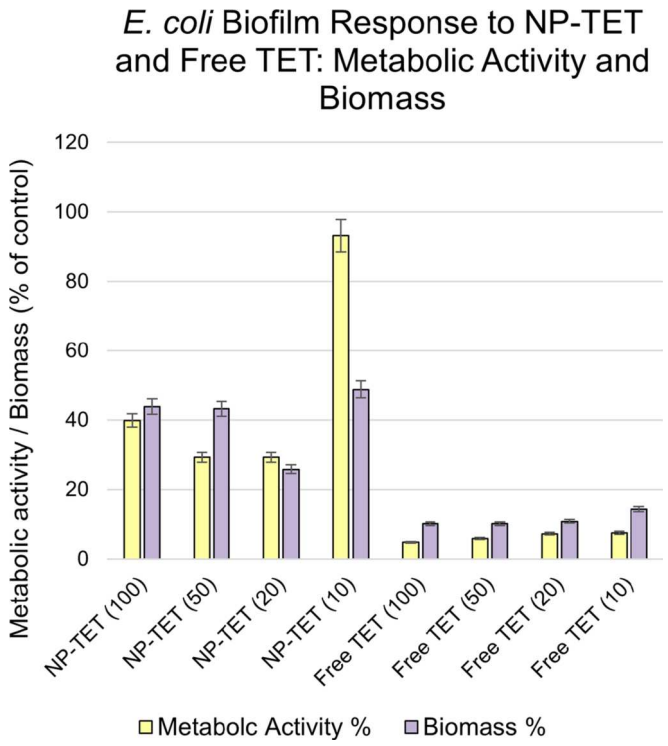

Figure 7. *E. coli* biofilm response to NP-TET and free TET treatments. Relative metabolic activity and biomass were evaluated after 24 h exposure to tetracycline-equivalent concentrations of 10–100 μg ml^{-1}. Metabolic activity was measured using the XTT assay, and biofilm biomass was quantified by crystal violet (CV) staining. Data are expressed as percentages relative to untreated control biofilms (set as 100%), where lower values indicate inhibition of biofilm growth or metabolic activity. Error bars represent mean ± SD from triplicate measurements.

metabolic inhibition than free tetracycline. At 5 μg ml^{-1} (measured but not plotted for clarity), NP-TET exhibited an anomalous increase in metabolic activity (324.6 ± 22.4%), suggesting a possible sub-inhibitory or stimulatory effect at very low dose.

Crystal violet staining demonstrated a similar concentration-dependent effect on total biomass (figure 6). Biomass levels were reduced to 62.85 ± 3.95%, 59.23 ± 3.41%, 67.58 ± 5.21%, and 49.56 ± 3.07% for NP-TET at 100, 50, 20, and 10 μg ml^{-1}, respectively. Free tetracycline treatments yielded biomass values of 37.49 ± 3.44%, 46.23 ± 3.22%, 33.37 ± 2.67%, and 32.48 ± 2.81%, indicating greater biomass reduction than NP-TET across the tested range. At 5 μg ml^{-1}, biomass reduction was minimal (52.2 ± 3.7%), confirming the reduced antibiofilm efficacy under sub-inhibitory conditions.

These results indicate that both formulations exerted antibiofilm effects against *S. aureus*, with NP-TET demonstrating enhanced metabolic inhibition at intermediate concentrations, while free tetracycline achieved stronger biomass disruption across the tested doses.

3.7.2. E. coli *biofilms*

As shown in figure 7, NP-TET treatment resulted in a concentration-dependent reduction in metabolic activity at higher concentrations. NP-TET at 100 and 50 μg ml^{-1} reduced metabolic activity to 39.87 ± 2.10% and 29.26 ± 2.53%, respectively, with a comparable reduction observed at 20 μg ml^{-1} (29.26 ± 2.71%). At 10 μg ml^{-1}, metabolic activity increased to 93.17 ± 5.97%, and at 5 μg ml^{-1} (measured but not plotted for clarity), a further rise to 123.10 ± 8.56% was detected, indicating a possible sub-inhibitory or adaptive response at very low concentration. In contrast, free tetracycline consistently produced stronger inhibition across all tested concentrations, yielding metabolic activities of 4.83 ± 0.30%, 5.94 ± 0.35%, 7.31 ± 0.42%, and 7.54 ± 0.41% at 100, 50, 20, and 10 μg ml^{-1}, respectively.

Biofilm biomass quantification followed a similar pattern. NP-TET treatment reduced biomass to 43.90 ± 3.48%, 43.24 ± 3.36%, and 25.83 ± 2.13% at 100, 50, and 20 μg ml^{-1}, while at 10 and 5 μg ml^{-1}, biomass values were higher (48.78 ± 4.75% and 41.46 ± 3.29%, respectively). Free tetracycline again produced a stronger reduction, yielding biomass levels of 10.20 ± 0.86%, 10.20 ± 0.86%, 10.86 ± 0.91%, and 14.41 ± 1.12% at 100, 50, 20, and 10 μg ml^{-1}, respectively.

Overall, both NP-TET and free tetracycline significantly reduced *E. coli* biofilm metabolic activity and biomass in a concentration-dependent manner at higher doses. However, NP-TET exhibited diminished efficacy

at 10 and 5 $\mu g\ ml^{-1}$, consistent with sub-inhibitory behavior at very low concentrations, whereas free tetracycline maintained strong and consistent inhibitory effects throughout the tested range.

4. Discussion

The microfluidic approach employed in this study enabled enhanced control over the assembly of chitosan–tripolyphosphate (TPP) nanoparticles compared to conventional batch methods. Precise manipulation of flow rates and micrometre-scale channel architecture facilitated rapid and homogeneous mixing during ionic gelation, supporting consistent nanoparticle nucleation and growth. This controlled environment yielded nanoparticles with narrow size distributions (PDI as low as 0.16) and tuneable surface charge, in line with the size uniformity and reproducibility advantages reported for microfluidic polyelectrolyte complexation systems [10, 19, 20]. Furthermore, the microfluidic process required minimal reagent volumes and offered scalability through modular design, making it suitable for both optimization and downstream translation.

The custom-designed chip architecture, which includes three mixing chambers followed by a serpentine region with periodic expansion zones, was optimized to maintain laminar flow and enhance passive, diffusion-driven mixing. These conditions supported efficient crosslinking between the cationic chitosan chains and anionic TPP, yielding nanoparticles with favourable colloidal stability and physicochemical properties relevant to drug encapsulation. Notably, the use of microfluidic confinement allowed for precise adjustment of residence time, which directly influenced particle morphology and charge, both of which are known to impact biological interactions with biofilms and tissue environments [21].

The fabrication of reproducible, leak-free PDMS microfluidic devices provided a robust platform for nanoparticle synthesis under controlled flow conditions. Soft lithography combined with oxygen plasma bonding enabled rapid prototyping and consistent device performance throughout the study. This fabrication reliability translated into process-level precision, supporting spherical nanoparticles formation. The resulting control over macromolecular assembly reinforces the potential of microfluidic systems for engineering chitosan-based nanocarriers with properties tailored for therapeutic delivery.

Systematic variation of the chitosan phase pH, CS:TPP flow ratio, and total flow rate influenced nanoparticle size and surface charge, indicating that these parameters affect the physicochemical characteristics of the resulting particles. The observed size dispersion can be attributed to pH-dependent protonation of chitosan and the CS:TPP stoichiometry under microfluidic mixing [22]. At a fixed CS:TPP flow ratio of 2:1, increasing pH from 4.5 to 5.0 reduced the Z-average from 257 nm (N1) to 132 nm (N4)—a ~49% decrease—consistent with moderated ionic crosslinking and controlled particle growth at partial protonation. A further increase to pH 5.5 resulted in slightly larger particles (159 nm, N7), indicating an optimum around pH 5.0 for this formulation. At a fixed pH of 5.0, decreasing the CS:TPP ratio from 2:1 to 1.5:1 or 1.25:1 increased particle size from 132 nm (N4) to 210 nm (N5) and 193 nm (N6), corresponding to ~59% and ~46% increases, respectively. This trend reflects the reduced positive charge density and weaker electrostatic stabilization that occur when chitosan is not in excess.

The optimized N4 formulation yielded nanoparticles with a hydrodynamic diameter of 132 ± 3 nm, a low polydispersity index (0.178 ± 0.004), and a surface charge of $+15.8 \pm 0.3$ mV, indicative of good colloidal stability. These properties compare favourably to batch-synthesized chitosan–TPP nanoparticles reported by Des Bouillons-Gamboa *et al* [22], which exhibited larger sizes (178–205 nm) and higher PDI values (0.47–0.56) under similar formulation conditions. Both studies observed aggregation under TPP-excess conditions, underscoring the formulation sensitivity inherent to ionic gelation systems. The inclusion of D-mannitol as a cryoprotectant during freeze-drying may have further contributed to post-lyophilization stability, highlighting the compatibility of microfluidic synthesis with downstream processing requirements for biomedical nanocarriers.

Similar formulation-dependent trends were reported by Gutiérrez-Ruíz *et al* [8],who demonstrated that variations in pH and CS:TPP ratio significantly influenced nanoparticle size, PDI, and zeta potential in batch-synthesized systems, with optimized particles measuring ~188 nm and a PDI of 0.16 ± 0.002. While their approach relied on surfactants and dialysis-based purification, the present microfluidic strategy produced similarly uniform or smaller nanoparticles without surfactant use. These findings highlight that formulation parameters and process conditions play a key role in shaping chitosan–TPP nanoparticle properties relevant to biomedical applications.

Morphological and structural analyses further confirmed successful nanoparticle formation and drug incorporation. SEM imaging showed that the optimized N4 formulation produced well-dispersed, quasi-spherical particles with smooth surface morphology and sub-150 nm dimensions, consistent with DLS measurements. Minor variations in the SEM micrographs are attributed to particle aggregation and flattening during the drying and solvent-evaporation steps required for imaging, which can slightly distort apparent size

uniformity compared with the hydrated state measured by DLS. In contrast, the raw chitosan powder exhibited irregular, flake-like structures lacking nanoscale definition, confirming the transformation of bulk polymer into discrete nanoparticles via microfluidic ionic gelation. FTIR spectroscopy supported these observations by revealing characteristic $-NH_3^+$ stretching and P–O bending bands in blank nanoparticles, indicative of effective ionic crosslinking. Following tetracycline loading, additional absorption bands at 1480, 1070, and 876 cm^{-1}—corresponding to aromatic ring vibrations and C–O skeletal modes—along with shifts in the N–H bending region, further substantiated drug encapsulation. These spectral features, absent in raw chitosan and blank particles, are consistent with previous reports on chitosan–drug nanoparticle systems [7]. The chitosan–TPP nanoparticles synthesized here are dense ionically crosslinked complexes, with stability best reflected by size, PDI, and zeta potential, while degradation is expected to occur mainly through enzymatic cleavage and ionic dissociation [22, 23].

Several studies have reported tetracycline–chitosan formulations produced by bulk methods. Shen *et al* developed tripolyphosphate–chitosan sponges that released tetracycline over ~11 days and retained antimicrobial activity against *S. aureus* and *E. coli* [24]. El-Alfy *et al* prepared tetracycline-, gentamycin-, and ciprofloxacin-loaded chitosan nanoparticles by ionic gelation and applied them to cotton and polyester fabrics to enhance antibacterial properties, although the particles displayed heterogeneous morphology and were primarily tested for surface finishing [25]. More recently, Ervina *et al* investigated chitosan nanoparticles containing 0.7% tetracycline for subgingival delivery in a rat periodontitis model, demonstrating reductions in probing depth and bleeding on probing as well as transient increases in FGF-2 expression [26]. Compared with these bulk-fabricated systems, the microfluidic approach described here yields nanoparticles with narrower size distributions and higher reproducibility, while requiring smaller reagent volumes. Importantly, their performance was evaluated directly against *S. aureus* and *E. coli* biofilms, providing infection-relevant validation that extends beyond surface coatings or periodontal regeneration models. These comparisons highlight the advantages of the microfluidic system in nanoparticle uniformity and biofilm applicability, while also underscoring formulation-specific aspects such as encapsulation efficiency.

The relatively low encapsulation efficiency (EE%) observed for tetracycline in this study can be attributed to its distinct molecular characteristics and its interaction with chitosan during nanoparticle formation. Tetracycline is a small, highly water-soluble molecule (log P ≈ -1.25) with a molecular weight of 444.4 g mol^{-1} and multiple ionizable functional groups, including phenolic, enolic, amide, and dimethylamino moieties [27, 28]. Its tricarbonyl system, along with three relevant pKa values (3.3, 7.7, and 9.7), causes it to exist predominantly in a cationic or zwitterionic form under the acidic conditions required for chitosan solubilization and nanoparticle synthesis [27]. At pH levels below 6.5, both tetracycline and chitosan carry net positive charges, resulting in electrostatic repulsion that hinders strong drug–polymer association during ionic gelation. Additionally, tetracycline's low molecular weight and high aqueous solubility favour its rapid diffusion into the external phase during nanoparticles formation, further limiting its entrapment within the polymer matrix. These combined factors explain the modest EE% (35%) observed for tetracycline-loaded chitosan–TPP nanoparticles, consistent with previously reported challenges in encapsulating small, hydrophilic, and highly ionizable drugs using ionic gelation-based systems [6, 29].

The observed differences in antibiofilm efficacy between NP-TET and free tetracycline highlight important considerations regarding nanoparticle-based antibiotic delivery. The comparatively lower suppression of biofilm biomass by NP-TET at equivalent doses, particularly at lower concentrations, may be attributed to the sustained-release behaviour and limited initial burst of the encapsulated drug, which is a common characteristic of polymeric nanoparticle systems targeting biofilms [30, 31].

In the case of *E. coli*, the denser extracellular polymeric matrix and species-specific biofilm architecture may have further restricted the diffusion of tetracycline from the nanoparticles, consistent with prior reports on nanoparticle penetration limitations in Gram-negative biofilms [32]. In contrast, metabolic inhibition in *S. aureus* biofilms was greater at intermediate NP-TET concentrations compared to free drug, suggesting that under certain dosing conditions, nanoparticle delivery may enhance biofilm suppression. However, at the lowest concentration tested (5 μg ml^{-1}), NP-TET induced an unexpected increase in metabolic activity, exceeding control levels. Control experiments with blank chitosan–TPP nanoparticles at equivalent concentrations showed no significant reduction in biofilm biomass or metabolic activity (Supplementary figures S1 and S2); in some cases, a slight increase in metabolic activity was observed, consistent with recently reported sub-inhibitory effects of cationic chitosan nanoparticles [33]. These results confirm that the antibiofilm activity originates from the tetracycline payload.

This observation is in line with reports of biofilm stimulation in response to sub-inhibitory antibiotic exposure. For example, Elawady *et al* (2024), sub-MIC exposure can enhance biofilm biomass and metabolic activity in *S. aureus*, possibly through stress-induced physiological adaptations, increased extracellular matrix production, or shifts in gene expression favouring biofilm development [34]. These findings emphasize the need for careful optimization of nanoparticle drug loading, release profiles, and dosing regimens when designing

chitosan-based antibiofilm therapeutics. Future work incorporating kinetic release studies, biofilm penetration assessments, and transcriptional analysis of stress-response genes could further clarify the mechanisms underlying these species-dependent responses. Although release kinetics were not examined here, drug-loaded chitosan–TPP nanoparticles are typically reported to exhibit biphasic release with an initial burst phase followed by sustained release [6, 29]. Future work will include detailed kinetic studies to confirm this behaviour in microfluidic-prepared formulations.

Overall, this study demonstrates the successful development of a microfluidic-based platform for the synthesis of size-controlled, tetracycline-loaded chitosan–TPP nanoparticles with confirmed drug loading and concentration-dependent antibiofilm activity. The combination of microfluidic process control, optimized formulation parameters, and effective biofilm inhibition highlights the potential of this system for future antimicrobial applications. Further investigations into drug release behaviour, biocompatibility, and broader antimicrobial efficacy will help advance the translational potential of this nanoparticle platform.

5. Conclusions

This work presents a microfluidic platform for the reproducible synthesis of tetracycline-loaded chitosan–TPP nanoparticles with consistent nanoscale characteristics. The custom passive micromixer facilitated controlled ionic crosslinking under continuous flow, producing colloidal nanocarriers whose size and surface charge could be adjusted by formulation conditions. Compared to conventional batch methods, the microfluidic approach enabled more consistent nanoparticle formation and improved reproducibility, even when encapsulating a small, hydrophilic antibiotic with known formulation challenges. The resulting nanocarriers exhibited concentration-dependent antibiofilm activity against both *Staphylococcus aureus* and *Escherichia coli*, demonstrating their relevance for localized antimicrobial applications. This study underscores the potential of flow-based nanomanufacturing strategies for engineering functional biomaterials and sets the stage for future integration with responsive or targeted delivery systems for infection-prone environments.

Conflict of interest

The authors declare no competing financial or non-financial interests.

Funding statement

This research did not receive any specific grant from funding agencies in the public, commercial, or not-for-profit sectors.

Ethics statement

This study did not involve human participants, animal experiments, or the use of human data or tissue. Therefore, ethical approval was not required.

Data availability statement

All data that support the findings of this study are included within the article (and any supplementary files).

Author contributions

Adei Abouhagger 0009-0004-0446-5769
Conceptualization (lead), Data curation (equal), Investigation (equal), Methodology (equal), Visualization (lead), Writing – original draft (lead), Writing – review & editing (lead)

Samanta Gelumbickytė 0009-0008-9123-1467
Data curation (equal), Investigation (equal), Methodology (equal), Writing – original draft (equal)

Monika Kirsnytė
Conceptualization (equal), Investigation (equal), Resources (equal)

Tatjana Kavleiskaja 0000-0002-2938-8550
Conceptualization (equal), Resources (equal), Validation (equal), Writing – review & editing (equal)

Arunas Stirkė 0000-0002-8081-3487
Funding acquisition (equal), Project administration (equal), Resources (equal), Supervision (equal), Writing – review & editing (equal)

Wanessa C M A Melo 0000-0002-5355-6155
Conceptualization (equal), Funding acquisition (equal), Investigation (equal), Project administration (equal), Resources (equal), Supervision (equal), Writing – review & editing (equal)

References

[1] Aswathanarayan J B, Rao P, Hm S, Gs S and Rai R V 2022 Biofilm-associated infections in chronic wounds and their management *Advances in Microbiology, Infectious Diseases and Public Health* (*in Advances in Experimental Medicine and Biology*) vol. 1434 ed G Donelli (Springer International Publishing) 55–75
[2] Yin W, Wang Y, Liu L and He J 2019 Biofilms: the microbial 'protective clothing' in extreme environments *IJMS* **20** 3423
[3] Finazzi S *et al* 2022 Tissue penetration of antimicrobials in intensive care unit patients: a systematic review—part I *Antibiotics* **11** 1164
[4] Birk S E, Boisen A and Nielsen L H 2021 Polymeric nano- and microparticulate drug delivery systems for treatment of biofilms *Adv. Drug Delivery Rev.* **174** 30–52
[5] Jia F, Gao Y and Wang H 2022 Recent advances in drug delivery system fabricated by microfluidics for disease therapy *Bioengineering* **9** 625
[6] Janes K A, Fresneau M P, Marazuela A, Fabra A and Alonso M J 2001 Chitosan nanoparticles as delivery systems for doxorubicin *J. Controlled Release* **73** 255–67
[7] Negi A and Kesari K K 2022 Chitosan nanoparticle encapsulation of antibacterial essential oils *Micromachines* **13** 1265
[8] Gutiérrez-Ruíz S C *et al* 2024 Optimize the parameters for the synthesis by the ionic gelation technique, purification, and freeze-drying of chitosan-sodium tripolyphosphate nanoparticles for biomedical purposes *J. Biol. Eng.* **18** 12
[9] Shrimal P, Jadeja G and Patel S 2020 A review on novel methodologies for drug nanoparticle preparation: Microfluidic approach *Chem. Eng. Res. Des.* **153** 728–56
[10] Niculescu A-G, Chircov C, Bîrcă A C and Grumezescu A M 2021 Nanomaterials synthesis through microfluidic methods: an updated overview *Nanomaterials* **11** 864
[11] Gimondi S, Ferreira H, Reis R L and Neves N M 2023 Microfluidic devices: a tool for nanoparticle synthesis and performance evaluation *ACS Nano* **17** 14205–28
[12] Ahmed M and Lu Y 2025 Synthesis of chitosan nanoparticles via microfluidic approach: the role of temperature in tailoring aggregation for enhanced uniformity *Micromachines* **16** 642
[13] Fonseca D R *et al* 2024 One-pot microfluidics to engineer chitosan nanoparticles conjugated with antimicrobial peptides using 'photoclick' chemistry: validation using the gastric bacterium *Helicobacter pylori ACS Appl. Mater. Interfaces* **16** 14533–47
[14] Maurizii G *et al* 2024 Non-invasive peptides delivery using chitosan nanoparticles assembled via scalable microfluidic technology *Carbohydrate Polymer Technologies and Applications* **7** 100424
[15] Soheili S, Mandegar E, Moradikhah F, Doosti-Telgerd M and Javar H A 2021 Experimental and numerical studies on microfluidic preparation and engineering of chitosan nanoparticles *J. Drug Delivery Sci. Technol.* **61** 102268
[16] Kumar Trivedi M 2015 Spectroscopic characterization of chloramphenicol and tetracycline: an impact of biofield treatment *Pharm. Anal. Acta* **06**
[17] Rivera Aguayo P *et al* 2020 Antimicrobial and antibiofilm capacity of chitosan nanoparticles against wild type strain of pseudomonas sp. isolated from milk of cows diagnosed with bovine mastitis *Antibiotics* **9** 551
[18] El-Naggar N E-A, Dalal S R, Zweil A M and Eltarahony M 2023 Artificial intelligence-based optimization for chitosan nanoparticles biosynthesis, characterization and *in-vitro* assessment of its anti-biofilm potentiality *Sci Rep.* **13** 4401
[19] Cabeza V S 2016 High and efficient production of nanomaterials by microfluidic reactor approaches *Advances in Microfluidics - New Applications in Biology, Energy, and Materials Sciences* ed X-Y Yu (InTech) (https://doi.org/10.5772/64347)
[20] Ma J, Lee S M-Y, Yi C and Li C-W 2017 Controllable synthesis of functional nanoparticles by microfluidic platforms for biomedical applications—a review *Lab Chip* **17** 209–26
[21] Danaei M *et al* 2018 Impact of particle size and polydispersity index on the clinical applications of lipidic nanocarrier systems *Pharmaceutics* **10** 57
[22] Des Bouillons-Gamboa R E *et al* 2024 Synthesis of chitosan nanoparticles (CSNP): effect of CH-CH-TPP ratio on size and stability of NPs *Front. Chem.* **12** 1469271
[23] Babaei-Ghazvini A, Acharya B and Korber D R 2021 Antimicrobial biodegradable food packaging based on chitosan and metal/metal-oxide bio-nanocomposites: a review *Polymers* **13** 2790
[24] Shen E, Wang C, Fu E, Chiang C, Chen T and Nieh S 2008 Tetracycline release from tripolyphosphate–chitosan cross-linked sponge: a preliminary *in vitro* study *J. of Periodontal Research* **43** 642–8
[25] El-Alfy E A, El-Bisi M K, Taha G M and Ibrahim H M 2020 Preparation of biocompatible chitosan nanoparticles loaded by tetracycline, gentamycin and ciprofloxacin as novel drug delivery system for improvement the antibacterial properties of cellulose based fabrics *Int. J. Biol. Macromol.* **161** 1247–60
[26] Silvia *et al* 2024 Effectiveness of chitosan nanoparticle containing 0.7% tetracyclines on clinical parameters and fibroblast growth: factor-2 in rat models *Int. J. App. Pharm.* 43–50 (https://journals.innovareacademics.in/index.php/ijap/article/view/51604)
[27] Udalova A Y, Dmitrienko S G, Natchuk S V, Apyari V V and Zolotov Y A 2015 Preconcentration of tetracycline antibiotics on a hyper-crosslinked polystyrene and their determination in waters by high-performance liquid chromatography *J. Anal. Chem.* **70** 292–7
[28] Li Z, Jiang H, Wang X, Wang C and Wei X 2023 Effect of pH on adsorption of tetracycline antibiotics on graphene oxide *IJERPH* **20** 2448
[29] Abosabaa S A, ElMeshad A N and Arafa M G 2021 Chitosan nanocarrier entrapping hydrophilic drugs as advanced polymeric system for dual pharmaceutical and cosmeceutical application: a comprehensive analysis using box-behnken design *Polymers* **13** 677

[30] Cao J et al 2023 Construction of nano slow-release systems for antibacterial active substances and its applications: a comprehensive review Front. Nutr. 10 1109204
[31] Serna N et al 2023 Efficient delivery of antimicrobial peptides in an innovative, slow-release pharmacological formulation Pharmaceutics 15 2632
[32] Fulaz S, Vitale S, Quinn L and Casey E 2019 Nanoparticle–biofilm interactions: the role of the EPS matrix Trends in Microbiology 27 915–26
[33] Maršík D, Maťátková O, Kolková A and Masák J 2024 Exploring the antimicrobial potential of chitosan nanoparticles: synthesis, characterization and impact on Pseudomonas aeruginosa virulence factors Nanoscale Adv. 6 3093–105
[34] Elawady R, Aboulela A G, Gaballah A, Ghazal A A and Amer A N 2024 Antimicrobial Sub-MIC induces Staphylococcus aureus biofilm formation without affecting the bacterial count BMC Infect Dis. 24 1065